iScience

CellPress

Article

Neuronal Receptors Display Cytoskeleton-Independent Directed Motion on the Plasma Membrane

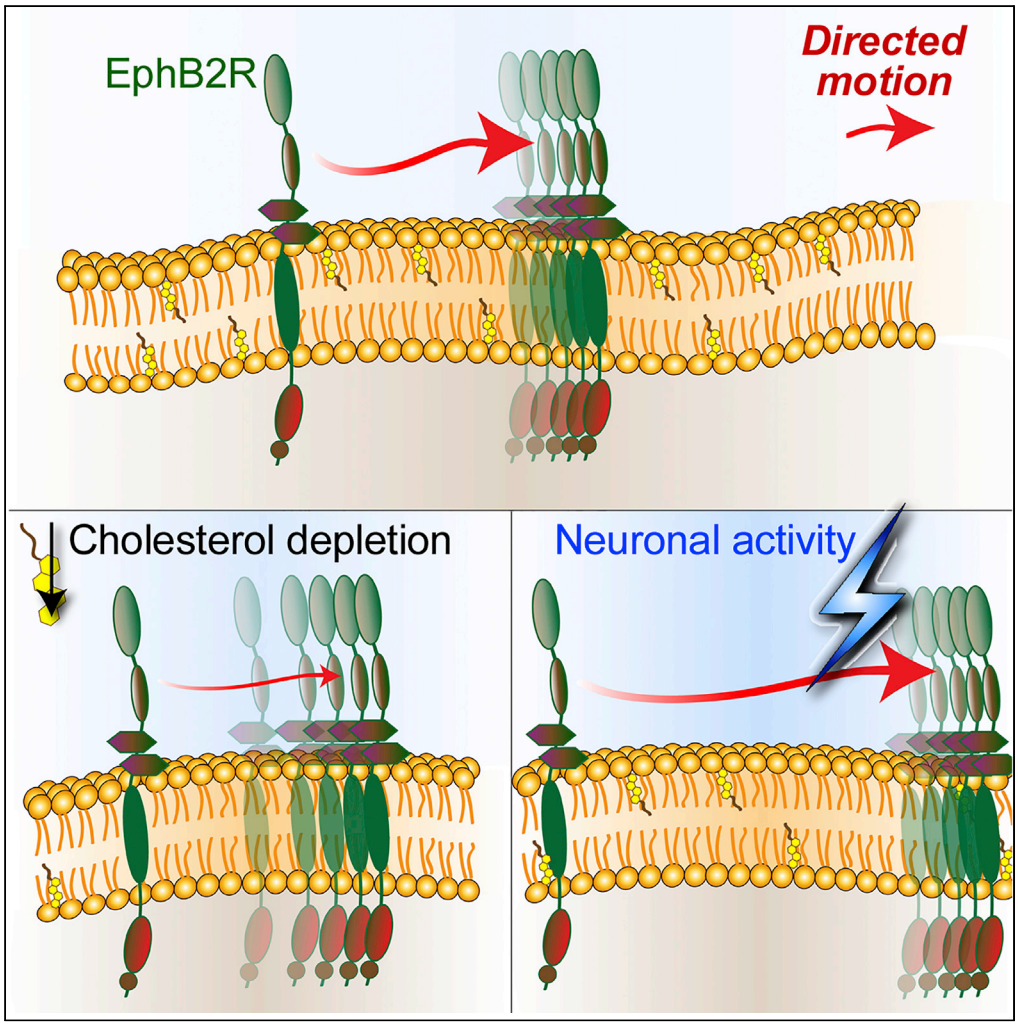

Ruth D. Taylor, Martin Heine, Nigel J. Emptage, Laura C. Andreae

nigel.emptage@pharm.ox.ac.uk (N.J.E.)
laura.andreae@kcl.ac.uk (L.C.A.)

HIGHLIGHTS

pH-sensitive quantum dot allows surface-specific single-particle tracking

EphB2 receptors undergo directed motion on the surface of neuronal membranes

Directed motion is dependent on membrane cholesterol but not the cytoskeleton

Directed motion occurs on dendrites between synapses and is activity dependent

Taylor et al., iScience *10*, 234–244
December 21, 2018
https://doi.org/10.1016/j.isci.2018.12.001

iScience

CellPress

Article

Neuronal Receptors Display Cytoskeleton-Independent Directed Motion on the Plasma Membrane

Ruth D. Taylor,[1,2] Martin Heine,[3,4,5] Nigel J. Emptage,[6,*] and Laura C. Andreae[1,2,7,*]

SUMMARY

Directed transport of transmembrane proteins is generally believed to occur via intracellular transport vesicles. However, using single-particle tracking in rat hippocampal neurons with a pH-sensitive quantum dot probe that specifically reports surface movement of receptors, we have identified a subpopulation of neuronal EphB2 receptors that exhibit directed motion between synapses within the plasma membrane itself. This receptor movement occurs independently of the cytoskeleton but is dependent on cholesterol and is regulated by neuronal activity.

INTRODUCTION

Receptor proteins that sit on the surface of the plasma membrane are critical for enabling cellular responses to the external environment. All cells need to be able to actively move these receptors from one location to another, often in a highly dynamic way. This directed movement is believed to be carried out by an elaborate system involving internalization of receptors by endocytosis into specialized transport vesicles, travel along the cytoskeletal network of the cell driven by molecular motors (Hirokawa and Takemura, 2005; Kapitein et al., 2010), and subsequent re-exocytosis into the destination location in the membrane. This transport is especially important in highly polarized cells such as neurons, where, for example, the rapid delivery of key receptors into and out of synapses can be critical for neuronal function. Indeed, the first description of a molecular motor that transports organelles along microtubules, kinesin, was in neuronal axons, where it mediated anterograde transport from the cell soma to neuron terminals, toward the plus end of microtubules (Vale et al., 1985).

In addition, membrane proteins exhibit lateral diffusion within the plasma membrane (Borgdorff and Choquet, 2002; Dahan et al., 2003; Heine et al., 2008; Kusumi et al., 1993). Lateral diffusion refers to the passive, random movement of proteins on the plasma membrane where they can move freely unless hindered sterically. This diffusional behavior was demonstrated using predominantly two main approaches: fluorescence recovery after photobleaching (FRAP) (Goehring et al., 2010) and single-particle tracking (SPT) (Triller and Choquet, 2008). FRAP experiments require the ensemble averaging of multiple molecules, whereas SPT allows tracking of individual proteins with a single fluorophore. The development of brightly fluorescent semiconductor nanoparticles, or quantum dots (QDs), with exceptional photostability and narrow emission spectra allowed accurate fluorophore localization (<10 nm) (Suzuki, 2012), long recording periods (>10 min), and improved color multiplexing in SPT. In neurons, the lateral diffusion of receptors can be restricted by membrane structures such as synapses and lipid rafts (Triller and Choquet, 2008). Furthermore, surface diffusion of these receptors and their recruitment into synapses are known to play important roles in synaptic plasticity and learning behavior (Choquet and Triller, 2013; Penn et al., 2017).

Overall, these findings have led to a current model where transmembrane proteins are believed to diffuse randomly in the plasma membrane but are transported in a directed manner within the cell via the movement of transport vesicles. However, it is not clear whether receptors might be able to undergo directed movement on the surface of the membrane. There is limited evidence that $GABA_A$ receptors may show this kind of behavior in neuronal growth cones (Bouzigues et al., 2007), but this was clearly entirely dependent on the microtubule network. In addition, given that QD-based probes are also able to report individual receptor switching between surface diffusion and intracellular active motor transport (Vermeheren-Schmaedick et al., 2014), a confident description of movement on the membrane surface requires surface-specific protein tracking. We now describe a specific pH-sensitive QD probe that can distinguish between surface membrane dynamics and intracellular transport. Using this probe, we adopted an SPT

[1]Centre for Developmental Neurobiology, Institute of Psychiatry, Psychology and Neuroscience, King's College London, London SE1 1UL, UK

[2]MRC Centre for Neurodevelopmental Disorders, King's College London, New Hunt's House, Guy's Campus, London SE1 1UL, UK

[3]Leibniz Institute of Neurobiology, Research Group Molecular Physiology, Brenneckestrasse 6, Magdeburg 39118, Germany

[4]Otto von Guericke University Magdeburg, Center for Behavioral Brain Sciences (CBBS), Universitätsplatz 2, Magdeburg 39106, Germany

[5]Johannes Gutenberg University Mainz, Institute for Developmental Biology and Neurobiology, AG Funktional Neurobiology, Hanns-Dieter-Hüsch Weg 15, Mainz 55128, Germany

[6]Department of Pharmacology, University of Oxford, Mansfield Road, Oxford OX1 3QT, UK

[7]Lead Contact

*Correspondence: nigel.emptage@pharm.ox.ac.uk (N.J.E.), laura.andreae@kcl.ac.uk (L.C.A.)

https://doi.org/10.1016/j.isci.2018.12.001

approach to track the transmembrane tyrosine kinase receptor, EphB2, a well-known neuronal protein with important roles in synapse formation (Sheffler-Collins and Dalva, 2012) and plasticity (Contractor et al., 2002; Grunwald et al., 2001), whose active intracellular transport along the cytoskeleton is important for dendritic arbor formation in neurons (Hoogenraad et al., 2005). We applied a sliding window analysis method to analyze the membrane surface trajectories, revealing directed motion of EphB2 receptors (EphB2Rs) on the cell surface of neuronal dendrites, occurring almost exclusively between synapses. This surface-directed motion was modulated by the cholesterol composition of the cell membrane but was insensitive to disruption of the cytoskeleton. To our knowledge, this is the first description of transmembrane protein movement on the cell surface by directed motion that is cell cytoskeleton independent. As both the lateral diffusion and intracellular vesicular transport of receptors in neurons are critical for synaptic and neuronal function, and hence regulated by activity (Anggono and Huganir, 2012; Bourke et al., 2018; Choquet and Triller, 2013; Park et al., 2004; Rumpel et al., 2005), we investigated the impact of activity on surface-directed motion. We found that neuronal activity promoted surface-directed movement of EphB2Rs.

RESULTS

Surface-Specific Tracking with a pH-Sensitive Quantum Dot

To specifically target single-molecule imaging to the cell surface, we were able to take advantage of a probe to differentiate between receptor movement on the neuronal cell surface and that within endosomal transport vesicles. The intraluminal (internal) environment of intracellular vesicles is relatively acidic (pH < 6) (Ouyang et al., 2013). We exploited our observation that the level of fluorescence emitted by the 655-nm-wavelength QD exhibited significant pH sensitivity. We labeled endogenous EphB2Rs in cultured neurons with the QD655 conjugate and examined the effect of changing the external pH. Bath application of pH 6 solution resulted in a dramatic quenching of QD fluorescence intensity to a level at which QDs could no longer be detected, whereas pH 7 solution had no effect (Figures 1A and 1B). As QD655 fluorescence is virtually undetectable at pH 6, this suggested that any visible QDs should reside on the neuronal surface, as those lying within vesicles would be effectively invisible. To verify that this was indeed the case, we used the membrane-impermeable dye, QSY-21, which is known to quench QD fluorescence (Jablonski et al., 2010). Addition of QSY-21 resulted in the inability to detect any QD-EphB2Rs within 10 s of its application (Figures 1C and 1D), further indicating that all visible QD-EphB2Rs are on the cell surface.

To confirm that intravesicular QD-labeled EphB2Rs are not detectable and to assess reversibility of quenching, we pre-treated neurons with clustered ephrinB1-Fc, a high-affinity ligand for EphB2Rs, which has been shown to cluster EphB2Rs and cause internalization to endosomes (Zimmer et al., 2003). If internal QD-EphB2Rs are present, but rendered undetectable by the relatively acidic endosomal environment, we reasoned that they should be revealed by neutralizing the endosomal pH gradient with ammonium chloride (NH_4Cl) (Axelsson et al., 2001; Miesenbock et al., 1998; Sankaranarayanan and Ryan, 2000). Upon addition of NH_4Cl, we saw a significant increase in the number of detected QD-EphB2Rs, compared with neurons that were treated with control Fc only (Figures 1E–1G). This unveiling of internalized QD-EphB2Rs further confirms that QD-EphB2Rs traveling within vesicles inside the cell are not visible and indicates that the pH-dependent quenching of QD655 is reversible. Taken together, these experiments demonstrate that all visible QD-EphB2Rs are located on the cell membrane surface.

EphB2Rs Show Directed Motion on the Surface of Neurons

SPT of surface QD-EphB2Rs in hippocampal neurons revealed that individual receptors are not static but move laterally in the neuronal cell membrane (Video S1 and Figure 2C). Standard approaches to the analysis of single-particle movement have utilized the mean squared displacement (MSD) method to distinguish between three types of motion displayed by particles: confined diffusion, free Brownian diffusion, and super-diffusive or "directed" motion. The method plots the MSD against the change in time between each "step" (δt) of the trajectory (Figure 2A) and determines two coefficients that describe the change in MSD. The diffusion coefficient (DC) is calculated over the linear portion (i.e., the first few points) of the function. The exponent α describes the curvature of the function and thus is an indicator of the type of motion displayed by the receptor, where $\alpha = 1$ represents diffusion, $\alpha < 1$ indicates confined diffusion, and $\alpha > 1$ indicates directed motion, and it is resolved over a longer timescale (Saxton and Jacobson, 1997) (Figure 2B). This type of analysis is generally applied over an entire trajectory and therefore assigns a single motion mode to each particle trajectory. However, we noticed that whereas some QD-EphB2Rs were either stationary or mobile for the duration of the recording, others interchanged between periods of relative

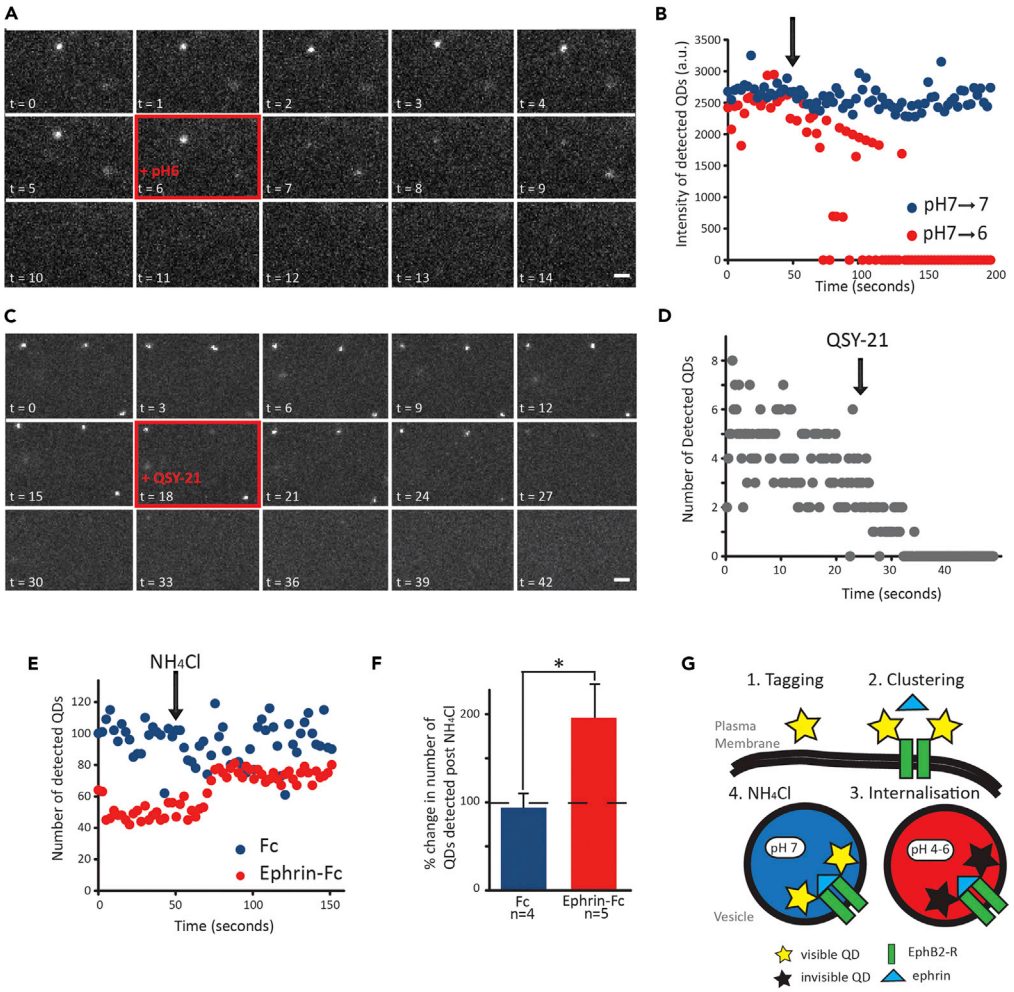

Figure 1. Single-Particle Tracking of EphB2Rs in Hippocampal Neurons with a Surface-Specific Quantum Dot Probe

(A and B) (A) Example time-lapse image series (in seconds) and (B) mean fluorescence intensities of QD-EphB2Rs following addition of pH 6 solution (red box in A, red circles in B) compared with pH 7 control (blue circles, B); scale bars, 2 μm.

(C and D) (C) Example time-lapse image series (in seconds) and (D) number of detected QD-EphB2Rs following addition of membrane-impermeable QSY-21 (100 μM) (red box in C).

(E and F) Dissipation of intracellular pH gradients by application of NH_4Cl (50 mM, pH 7.2) to neurons previously incubated with pre-clustered ephrinB1 (Ephrin-Fc; red circles, n = 5) or control Fc fragments (Fc; blue circles, n = 4) leads to a significant increase in detected QD-EphB2Rs in the former; (E) mean number of detected QD-EphB2Rs over time; and (F) quantification of change from baseline ($p < 0.05$, graph shows mean ± SEM).

(G) Model illustrating experiments shown in (E and F): clustering of QD-labeled EphB2Rs leads to receptor internalization and hence QD fluorescence quenching. These QD-EphB2Rs are then revealed by neutralization of pH.

localized stability and unrestricted motion (Video S1), suggesting that a more time-resolved analysis would be able to better describe individual trajectories. Indeed, segmenting trajectories by synaptic location has previously demonstrated that the diffusion characteristics of neurotransmitter receptors vary depending on whether they are located at or outside the synapse (Renner et al., 2012). We therefore analyzed the trajectories of QD-EphB2Rs by calculating MSD within sliding time windows, based on an approach previously validated in microtubule transport (Arcizet et al., 2008). This approach generates a (smoothed) plot of how each parameter (distance, DC, α) changes with time (Figures 2F–2I) and confirmed our impression that individual receptors exhibit varying DCs over the time course of a single trajectory (Figure 2G).

To distinguish between diffusive and directed motion, we set a very stringent threshold to define directed motion: as $\alpha > 1.56$ (see Methods). Nonetheless, to our surprise, we found that some receptors appeared to

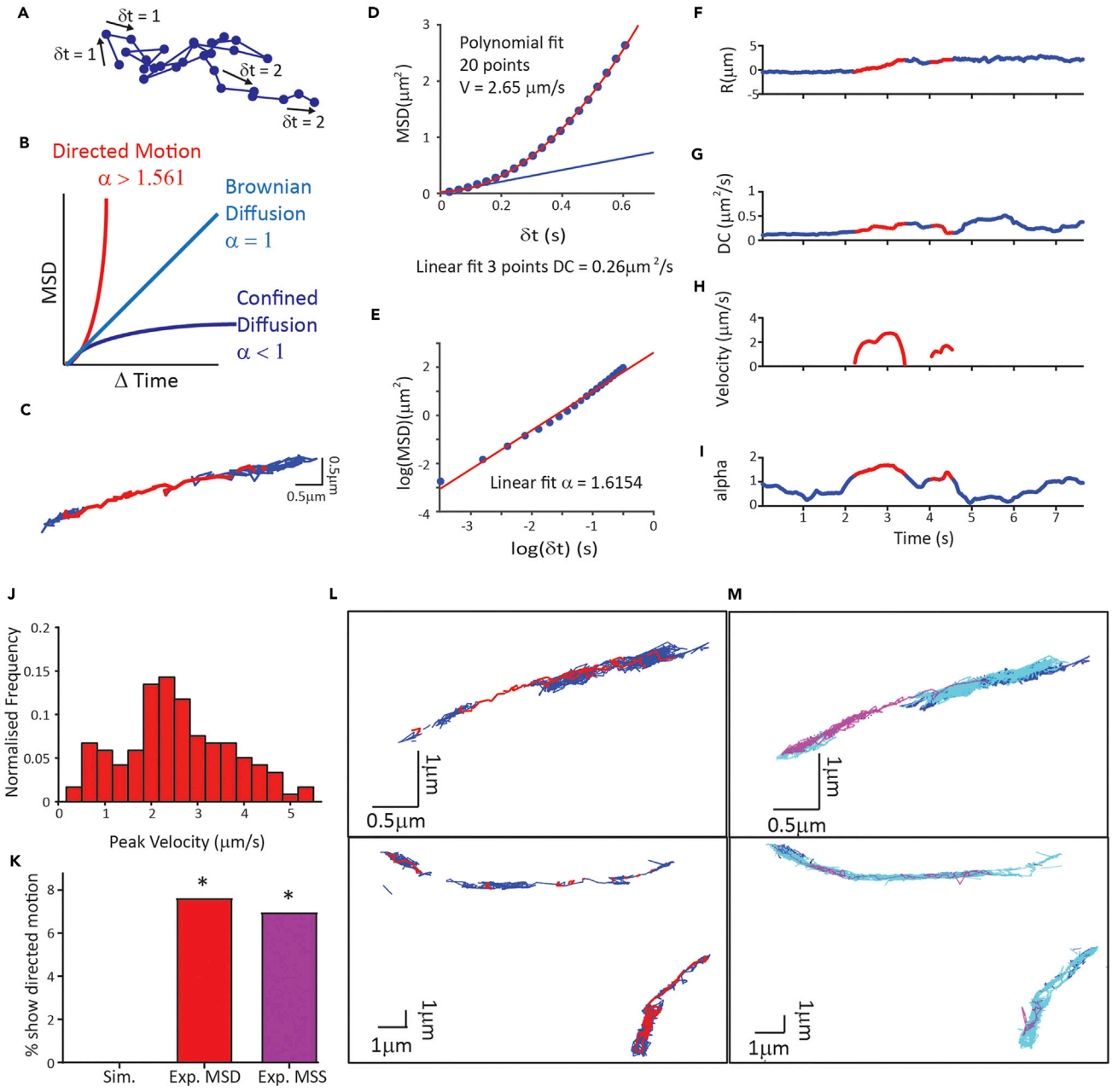

Figure 2. Analysis of QD-EphB2R Trajectories Reveals Directed Motion

(A) Model trajectory indicating δt.

(B) Traditional analysis plots MSD against Δt to obtain exponent, α, indicating motion type.

(C) Example QD-EphB2R trajectory. Colors represent motion modes with red indicating directed motion and blue illustrating diffusive motion. See also Video S1.

(D–I) Time resolved MSD analysis. (D) MSD plotted against time interval (δt) for illustrated trajectory during directed motion for a single "sliding" window (20 time points) yields a DC of 0.26 $\mu m^2/s$ by linear fit over the linear portion of the graph (blue line) and a velocity (V) of 2.65 μm/s when fitting a power equation to the full dataset (red curve). (E) A plot of log(MSD) against log(δt) for the same period yields alpha (α) of 1.6154 (slope of linear fit). (F–I) Time-resolved MSD analysis of the illustrated QD-EphB2R trajectory seen in (C) showing (F) displacement, (G) diffusion coefficient, (H) velocity, and (I) α varying over the time course of the trajectory; threshold for directed motion $\alpha > 1.561$.

(J) Frequency distribution of detected peak velocities in experimental data (n = 119; mean = 2.51 ± 1.16 μm/s).

(K) Quantification to compare percentage of experimental QDs showing directed motion with simulated data of Brownian motion (0/350), time-resolved MSD (red, 14/183, chi-square $p < 0.0001$), and DC-MSS (magenta, 34/452, chi-square $p < 0.0001$). See also Figure S1.

(L and M) Example trajectories of QD-EphB2Rs displaying similar segments of directed motion using (L) time-resolved MSD analysis and (M) DC-MSS analysis. Trajectories are color coded for motion mode depending on analysis: (L) for time-resolved MSD, directed motion is displayed in red and diffusion in blue, whereas (M) for DC-MSS, directed motion is in magenta, with diffusion in blue and confined diffusion in cyan.

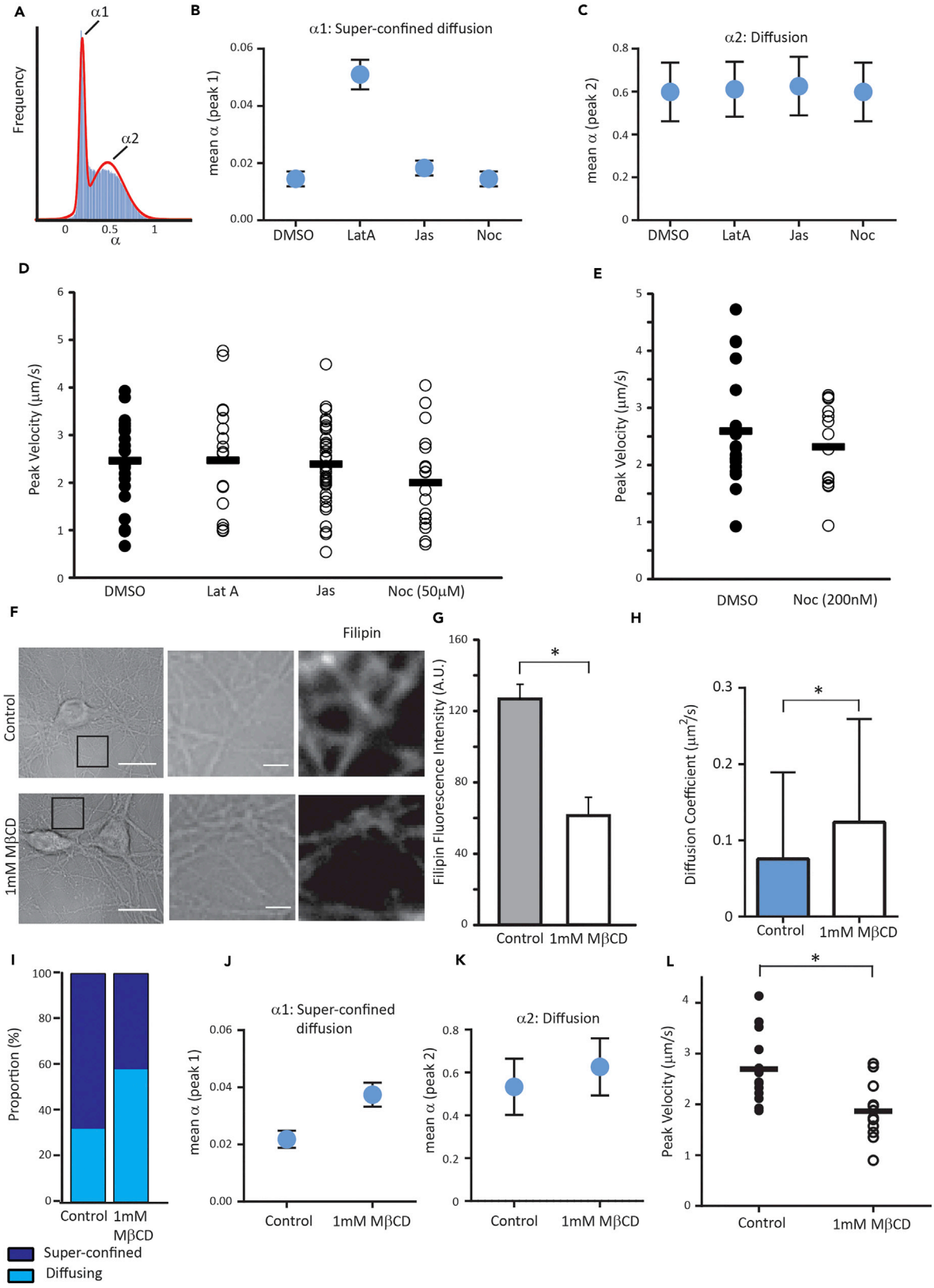
A
α1
α2
Frequency
α
B
α1: Super-confined diffusion
mean α (peak 1)
DMSO
LatA
Jas
Noc
C
α2: Diffusion
mean α (peak 2)
DMSO
LatA
Jas
Noc
D
Peak Velocity (μm/s)
DMSO
Lat A
Jas
Noc (50μM)
E
Peak Velocity (μm/s)
DMSO
Noc (200nM)
F
Filipin
Control
1mM MβCD
G
Filipin Fluorescence Intensity (A.U.)
Control
1mM MβCD
H
Diffusion Coefficient (μm²/s)
Control
1mM MβCD
I
Proportion (%)
Control
1mM MβCD
Super-confined
Diffusing
J
α1: Super-confined diffusion
mean α (peak 1)
Control
1mM MβCD
K
α2: Diffusion
mean α (peak 2)
Control
1mM MβCD
L
Peak Velocity (μm/s)
Control
1mM MβCD

Figure 3. Directed Motion of Surface EphB2Rs Is Not Affected by Cytoskeleton-Modifying Drugs but Is Dependent on Membrane Cholesterol

(A) Bimodal frequency distribution plot for values of instantaneous α in diffusing QD-EphB2Rs indicates a super-confined population (α_1) and a more freely diffusing population (α_2).

(B and C) The effect of modulating the actin cytoskeleton (Lat A: latrunculin A; 5 μM; Jas, jasplakinolide, 5 μM) or the microtubule network (Noc, nocodazole, 50 μM) on α_1 (B) and α_2 (C). Error bars represent standard deviation.

(D) Modifying the actin cytoskeleton or the microtubule network does not change the peak velocity of QD-EphB2Rs; bars indicate the mean; n = 18–40.

(E) As for (D), cells incubated in low-dose nocodazole.

(F and G) Treatment with 1 mM methyl-β-cyclodextrin (MβCD) reduces cholesterol levels; (F) left panels show representative bright-field images of dissociated neurons; scale bar, 10 μm, with higher-power views of bright-field images (middle) and filipin fluorescence (right) of selected regions; scale bar 2 μm. (G) Quantification of filipin fluorescence intensities; error bars represent SEM (control: n = 48 dendrites, MβCD: n = 49, $p < 0.05$).

(H–K) (H) Cholesterol depletion with MβCD significantly increases the instantaneous DC of diffusing QD-EphB2Rs (control: 0.075 $\mu m^2/s$, MβCD: 0.123 $\mu m^2/s$, $p < 0.05$). (I) MβCD treatment changes the relative proportions of diffusing QD-EphB2Rs that display super-confined versus freely diffusing characteristics (as defined by the value of instantaneous α), increases mean α_1 (J) and to a lesser degree, α_2 (K). (H–K) Error bars represent standard deviation.

(L) Peak velocity of QD-EphB2Rs is significantly reduced by MβCD (n = 13–17, $p < 0.05$, chi-square). See also Figure S2.

undergo short periods of directed motion (71/1,287) (Figures 2C–2E and 2I) with an average peak velocity of 2.51 ± 1.156 μm/s (Figure 2J). We compared experimental data (without blinks, see Methods) with time-resolved analysis of simulated trajectories of randomly moving particles displaying Brownian motion. We found that there was a significantly greater proportion of experimental EphB2R trajectories exhibiting periods of directed motion than of simulated ones, indeed with no such episodes arising from analysis of the simulated pure diffusional trajectories (experimental trajectories: 7.7%, 14/183; simulated Brownian trajectories: 0/350, chi-square test, $p < 0.0001$, Figure 2K). As further confirmation that these surface receptors exhibit directed motion, we employed a second validated approach to analyze QD-EphB2R trajectory data: divide-and-conquer motion scaling spectrum analysis (DC-MSS) (Vega et al., 2018). In summary, DC-MSS initially classifies the motion type by calculating the change in the maximum pairwise distance (MPD) between particle positions within a sliding window. Maxima in ΔMPD indicate a switch of motion modes enabling track segmentation. Once the trajectory has been segmented, the motion scaling spectrum is calculated for each segment of the trajectory as previously described (Ewers et al., 2005). Segments of trajectory that display directed motion analyzed by time-resolved MSD analysis (Figure 2L) similarly display directed motion in DC-MSS (Figure 2M), with a similar proportion of trajectories showing directed motion (7.5%, 34/452, Figure 2K).

To determine whether it might be possible to detect apparent directed motion as a result of the geometry of membrane space available for diffusion, we modeled diffusional movement of particles in a variety of spatially defined regions. In no case were we able to identify directed movement (see Figures S1A and S1B). Reduced sampling rates also only reduced the apparent α (Figure S1C). Since all labeled EphB2Rs in our experiments are restricted to the external neuronal surface, such that the episodes of directed motion cannot be due to intracellular vesicular transport, these results demonstrate that these receptors have the capacity to move with directed motion on the plasma membrane.

Diffusion of Surface EphB2Rs Is Restricted by Actin, whereas Directed Motion Is Cytoskeleton Independent but Depends on Membrane Cholesterol

We next asked to what extent either the diffusive or the directed motion of surface EphB2Rs is dependent on the cell cytoskeleton. We conducted QD-EphB2R tracking experiments in the presence of cytoskeleton-modifying drugs and compared their motion characteristics with vehicle control (DMSO). When we analyzed only those receptors undergoing diffusive motion (excluding all directed motion), we found that there were two populations of diffusing QD-EphB2Rs: super-confined (mean $\alpha = 0.026$) and diffusing (mean $\alpha = 0.59$) (Figure 3A). Recently, an extension of the fluid mosaic model describing cell membrane structure (Singer and Nicolson, 1972) has been proposed, which describes different compartments within a phospholipid-cholesterol sheet, supported by a meshwork of microtubules and actin filaments (Kusumi et al., 2011). This model envisages membrane structure as being composed of an actin-based "fence" and transmembrane protein "pickets." We speculated that movement of the super-confined group of receptors might be limited by this actin fence, and indeed, disruption of the actin cytoskeleton by addition of latrunculin A (5 μM) caused a significant increase in α (i.e., greater movement) of the super-confined group (Figure 3B) without affecting the more freely diffusing receptors (Figure 3C). No changes to α were seen following disruption of the microtubule network (Figures 3B and 3C). Similarly, latrunculin A caused a significant increase in the mean DC for both super-confined and diffusing receptors with an equivalent shift in the DC distribution (Figure S2). This is consistent with previous studies (Umemura et al., 2008), including of

other neuronal receptors (Rust et al., 2010). However, neither modulation of the actin cytoskeleton (depolymerization with latrunculin A or stabilization with jasplakinolide) nor the microtubule network (depolymerization with high-dose nocodazole or inhibition of microtubule dynamics with nocodazole at low dose; Jaworski et al., 2009) altered the directed motion characteristics of QD-EphB2Rs in terms of the peak velocity (Figures 3D and 3E), the proportion of QDs that show directed motion (DMSO: 8.57%, n = 315; jasplakinolide: 10.20%, n = 245; latrunculin A: 8.28%, n = 145; nocodazole: 7.76%, n = 245), or the time any given QD spent in directed motion mode (DMSO: 0.10 ± 0.01 s, n = 25; jasplakinolide: 0.11 ± 0.01 s, n = 40; latrunculin A: 0.14 ± 0.03 s, n = 18; nocodazole: 0.14 ± 0.03 s, n = 18).

We therefore hypothesized that the directed motion of EphB2Rs might be dependent in some way on the neuronal plasma membrane itself. Application of 1 mM methyl-β-cyclodextrin (MβCD) resulted in depletion of membrane cholesterol in neuronal processes by approximately 50%, as quantified by levels of the macrolide filipin, a cholesterol-binding fluorescent marker (Hering et al., 2003; Maxfield and Wustner, 2012; Renner et al., 2009) (Figures 3F and 3G). As previously reported (Renner et al., 2009), cholesterol depletion with MβCD resulted in an increase in DC that was accompanied by a change in the distribution of α (Figures 3H–3K). Although cholesterol depletion did not affect the proportion of QD-EphB2Rs displaying directed motion, it resulted in a significant reduction in the peak rate of directed motion (Figure 3L). This indicates that the directed movement of surface EphB2Rs is dependent on membrane cholesterol.

Directed Motion of EphB2Rs Occurs between Synapses and Is Activity Dependent

We then questioned whether the directed motion of EphB2Rs exhibited any spatial specificity. A key feature of the neuronal landscape is the presence of postsynaptic specializations at intervals along dendrites, which are known to affect receptor diffusion. For example, it has previously been shown that glutamatergic receptors show restricted diffusion within synapses and anomalous diffusion outside synapses (Groc et al., 2004; Heine et al., 2008). Using traditional immunostaining, we find EphB2Rs to be predominantly localized to dendrites, largely between synapses, in these cultures (Figure S3). To track QD-EphB2R movement relative to synapse position, we expressed PSD95-GFP in neurons, to label the postsynaptic compartment, and imaged QD-EphB2Rs. Figure 4A shows a representative trajectory of a QD-EphB2R in relation to PSD-95. In this example, whereas the QD-EphB2R clearly diffuses into the synaptic/perisynaptic compartment (blue), directed motion (red) is only seen outside this region. Quantification of trajectory segments showing diffusion versus directed motion demonstrates that EphB2Rs with a velocity are very rarely seen at the synapse (comprising synapse and perisynaptic area), compared with diffusing receptors (Figure 4B). These data indicate that surface EphB2Rs exhibit fast directed motion along dendrites and between postsynaptic specializations.

Finally, to determine whether this directed movement might be regulated by neuronal activity, we analyzed the directed motion characteristics of QD-EphB2Rs following electrical field stimulation. We found that QD-EphB2Rs travel for a longer duration in directed motion mode following stimulation with 900 action potentials at 20 Hz (mean duration prestimulation: 0.09 ± 0.05 s, mean duration 5 min post stimulation: 0.14 ± 0.09 s) without an associated change in peak velocity (peak velocity prestimulation: 2.40 ± 0.90 μm/s, peak velocity 5 min post stimulation: 2.52 ± 0.73 μm/s) (Figure 4C). Thus increased neuronal activity promotes rapid intersynaptic movement of surface EphB2Rs.

DISCUSSION

We propose that cholesterol-dependent "conduits" within the dendritic plasma membrane may allow brief spells of rapid surface receptor travel between synapses. Under conditions of increased neuronal activity, receptors spend longer in these conduits (model illustrated in Figure 4D).

In this study, we have used a pH-dependent QD probe to ensure that we have at all times tracked receptors localized to the neuronal plasma membrane. QDs have been described to show pH-dependent changes in fluorescent levels, including quenching at acidic pH (Debruyne et al., 2015; Gao et al., 2002), and have been used previously to examine synaptic vesicle recycling in neurons (Zhang et al., 2009). In the latter study, the QD605 (Fisher) was found to exhibit relatively small levels of quenching (~15%) at pH 5, although this was still sufficient to detect vesicle cycling. Here, we find that the QD655 exhibits much higher levels of pH sensitivity in this range, making it useful for a variety of biological applications. QD quenching in response to shifts in pH is known to be highly dependent on the nature of the organic coating surrounding

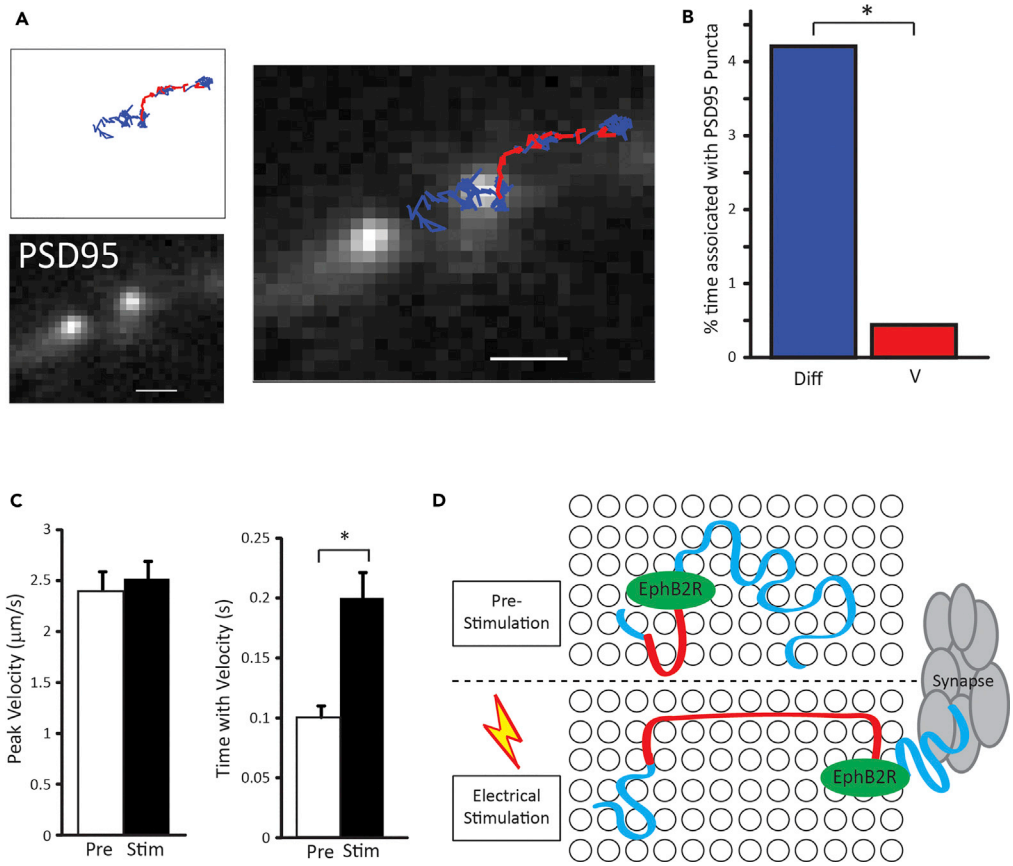

Figure 4. Directed Motion Is Spatially Restricted and Activity Dependent

(A) Representative trajectory of a single QD-EphB2R along a neuronal process expressing PSD-95-GFP to localize synapses (see also Figure S3). Regions of the trajectory in which the QD-EphB2R has an associated velocity/displays directed movement are illustrated in red, with diffusive movement in blue; scale bars, 1 μm.

(B) Percentage of time in which diffusing QD-EphB2Rs (Diff, dark blue) or those displaying directed motion (V, red) are associated with the peak of PSD-95-GFP puncta ($n = 41$, $p < 0.05$, chi-square).

(C) Field stimulation of the neuronal network increases time spent with a velocity, without changing the peak velocity.

(D) Proposed model for the movement of QD-EphB2Rs in the membrane before and after electrical stimulation. QD-EphB2Rs (shown in green) diffuse in the cell membrane (blue tracks) displaying directed motion (red tracks) for short periods of time. QD-EphB2Rs located near or at the synapse only display diffusive motion. After electrical stimulation, the QD-EphB2Rs spend a greater proportion of time undergoing directed motion. Error bars represent SEM.

the core-shell region, and although the specific coatings of both QD605 and QD655 are proprietary, it is likely that the differences in sensitivity are due to variations in this coating.

We have used two different analysis methods to identify directed motion, so our findings are unlikely to have arisen as a result of the analytical approach. However, a potential issue is that all trajectories were imaged in 2D, effectively projecting what is in reality 3D movement onto a 2D plane. Although neuronal processes grown in culture (without glia on the coverslip) represent an exceptionally flat system, we also minimized the impact of this by monitoring changes in the point spread function and excluding trajectories with greater than 15% change. Critically, however, projection from 3D to 2D results in a reduction in identified instances of directed motion (Dupont et al., 2013). We are therefore confident that directed motion is not over-represented in our system, and indeed may be under-represented.

Using electrical stimulation, we find that the directed motion of EphB2Rs is activity dependent, where increased activity results in receptors spending more time undergoing this form of motion, without changing overall speed. It is well known that activity can affect the diffusional movement of receptors in neuronal membranes (Choquet and Triller, 2013). Synaptic activation and elevations of intracellular calcium levels

can regulate the diffusion of dendritic AMPARs (Borgdorff and Choquet, 2002; Heine et al., 2008), predominantly in the extrasynaptic space (Groc et al., 2004). Similarly, activity affects the lateral diffusion of $GABA_A$ receptors in a calcium-dependent manner (Bannai et al., 2009; de Luca et al., 2017). Interestingly, the calcium-influx-dependent reduction in $GABA_A$ receptor DC is also restricted to dendritic regions between synapses, and this may provide a mechanism for transfer of an "activation memory" between inhibitory synapses (de Luca et al., 2017). Recently, tracking of intracellular transport vesicles has demonstrated that increased neuronal activity (via "chemical long-term potentiation" [cLTP]) resulted in elevated anterograde velocities of AMPARs undergoing directed movement in vesicles, in the later stages of cLTP (Hangen et al., 2018). It is apparent that neurons require methods to alter the distribution of key receptors in response to changes in activity levels and patterns, and directed membrane flow could represent an additional mechanism.

The dominant model of cell membrane structure remains the fluid mosaic model (Goni, 2014; Singer and Nicolson, 1972) where both proteins and lipids move within the fluid lipid bilayer, which is often described as having the consistency of olive oil (Edidin, 2003). This fluidity includes both translational and rotational (about their own axis) movement of molecules. In biological membranes, cholesterol is thought to "buffer" fluidity, increasing fluidity at lower temperatures and reducing it at higher ones (Alberts, 2015; Maxfield and van Meer, 2010). Cholesterol is also associated with a liquid ordered phase where rotational movement is restricted (Goni, 2014), possibly in the context of lipid nanodomains, or "rafts" (Simons and Ikonen, 1997; Simons and van Meer, 1988). Indeed, high-resolution live cell imaging studies have indicated that cholesterol plays a role in "trapping" sphingolipids and glycosylphosphatidylinositol (GPI)-anchored proteins (Dietrich et al., 2002; Suzuki et al., 2012; Wenger et al., 2007). Consistent with this, our finding of significant increases in mean values of α for both super-confined and confined diffusing EphBRs, together with the overall increase in DC, suggests release from such domains. Although manipulation of cholesterol levels can also have effects on the actin cytoskeleton (Goodwin et al., 2005; Kwik et al., 2003; Sun et al., 2007), including the organization of GPI-anchored proteins in the membrane (Goswami et al., 2008), and indeed actin-dependent, directional membrane flows have recently been described (Ashdown et al., 2017), the lack of effect on directed motion from modulation of the actin network argues that this is not actin mediated, but rather dependent on the membrane itself. A possibility is that highly transient fluid currents may provide the conduits for directional movement of proteins in the neuronal membrane. In a polarized cell such as a neuron, with the need to rapidly move proteins in response to stimuli such as activity, this could represent an alternative and energy-efficient method of protein delivery.

Limitations of the Study

This work was carried out *in vitro* using cultured rat neurons. Although it remains very challenging to perform SPT in mammalian neurons *in vivo*, especially where antibodies to specific proteins are used as here, it will be critical to devise new methods in the future to allow confirmation of findings in more intact preparations. In addition, the development of new, alternative probes, especially ones that can be genetically encoded and are smaller in size than those used here, will aid validation. We have discussed the limitations of imaging in 2D versus 3D in the Discussion section. Although we demonstrate the impact of cholesterol depletion on directed motion, it will be important to assess whether more subtle or different ways of changing or disrupting membrane lipids also affect this behavior.

METHODS

All methods can be found in the accompanying Transparent Methods supplemental file.

SUPPLEMENTAL INFORMATION

Supplemental Information includes Transparent Methods, three figures, and one video and can be found with this article online at https://doi.org/10.1016/j.isci.2018.12.001.

ACKNOWLEDGMENTS

The help of Daniel Choquet and the Bordeaux Imaging Center, part of the national infrastructure France-BioImaging, grant ANR-10INBS-04-0, is acknowledged. This research was supported by BBSRC grant BB/P000479/1 (to L.C.A.), MRC grant G0802613 (to N.J.E.), and the Sackler Institute for Translational Neurodevelopment (R.D.T.). L.C.A. is a NARSAD Young Investigator. We thank Richard Marsh and Susan Cox (Randall Center for Cell and Molecular Biophysics, KCL) and Eldad Afik (California Institute of Technology)

for technical help and advice; Uwe Drescher (KCL) for the kind gift of Fc fragments, ephrinB1-Fc, and antibodies against Fc; and Oscar Marin and members of the Andreae and Emptage laboratories for critical discussions.

AUTHOR CONTRIBUTIONS

Conceptualization, R.D.T., N.J.E., and L.C.A.; Methodology, R.D.T., M.H., N.J.E., and L.C.A.; Software, R.D.T.; Investigation R.D.T., M.H., and L.C.A.; Resources, N.J.E. and L.C.A.; Writing, R.D.T. and L.C.A.; Review & Editing, R.D.T., M.H., N.J.E., and L.C.A.; Funding acquisition, N.J.E. and L.C.A.

DECLARATION OF INTERESTS

The authors declare no competing interests.

Received: March 13, 2018
Revised: July 25, 2018
Accepted: November 30, 2018
Published: December 21, 2018

REFERENCES

Alberts, B. (2015). Molecular Biology of the Cell, Sixth Edition (Garland Science, Taylor and Francis Group).

Anggono, V., and Huganir, R.L. (2012). Regulation of AMPA receptor trafficking and synaptic plasticity. Curr. Opin. Neurobiol. *22*, 461–469.

Arcizet, D., Meier, B., Sackmann, E., Radler, J.O., and Heinrich, D. (2008). Temporal analysis of active and passive transport in living cells. Phys. Rev. Lett. *101*, 248103.

Ashdown, G.W., Burn, G.L., Williamson, D.J., Pandzic, E., Peters, R., Holden, M., Ewers, H., Shao, L., Wiseman, P.W., and Owen, D.M. (2017). Live-cell super-resolution reveals F-actin and plasma membrane dynamics at the T cell synapse. Biophys. J. *112*, 1703–1713.

Axelsson, M.A., Karlsson, N.G., Steel, D.M., Ouwendijk, J., Nilsson, T., and Hansson, G.C. (2001). Neutralization of pH in the Golgi apparatus causes redistribution of glycosyltransferases and changes in the O-glycosylation of mucins. Glycobiology *11*, 633–644.

Bannai, H., Levi, S., Schweizer, C., Inoue, T., Launey, T., Racine, V., Sibarita, J.B., Mikoshiba, K., and Triller, A. (2009). Activity-dependent tuning of inhibitory neurotransmission based on GABAAR diffusion dynamics. Neuron *62*, 670–682.

Borgdorff, A.J., and Choquet, D. (2002). Regulation of AMPA receptor lateral movements. Nature *417*, 649–653.

Bourke, A.M., Bowen, A.B., and Kennedy, M.J. (2018). New approaches for solving old problems in neuronal protein trafficking. Mol. Cell. Neurosci. *91*, 48–66.

Bouzigues, C., Morel, M., Triller, A., and Dahan, M. (2007). Asymmetric redistribution of GABA receptors during GABA gradient sensing by nerve growth cones analyzed by single quantum dot imaging. Proc. Natl. Acad. Sci. U S A *104*, 11251–11256.

Choquet, D., and Triller, A. (2013). The dynamic synapse. Neuron *80*, 691–703.

Contractor, A., Rogers, C., Maron, C., Henkemeyer, M., Swanson, G.T., and Heinemann, S.F. (2002). Trans-synaptic Eph receptor-ephrin signaling in hippocampal mossy fiber LTP. Science *296*, 1864–1869.

Dahan, M., Levi, S., Luccardini, C., Rostaing, P., Riveau, B., and Triller, A. (2003). Diffusion dynamics of glycine receptors revealed by single-quantum dot tracking. Science *302*, 442–445.

de Luca, E., Ravasenga, T., Petrini, E.M., Polenghi, A., Nieus, T., Guazzi, S., and Barberis, A. (2017). Inter-synaptic lateral diffusion of GABAA receptors shapes inhibitory synaptic currents. Neuron *95*, 63–69.e5.

Debruyne, D., Deschaume, O., Coutino-Gonzalez, E., Locquet, J.P., Hofkens, J., Van Bael, M.J., and Bartic, C. (2015). The pH-dependent photoluminescence of colloidal CdSe/ZnS quantum dots with different organic coatings. Nanotechnology *26*, 255703.

Dietrich, C., Yang, B., Fujiwara, T., Kusumi, A., and Jacobson, K. (2002). Relationship of lipid rafts to transient confinement zones detected by single particle tracking. Biophys. J. *82*, 274–284.

Dupont, A., Gorelashvili, M., Schuller, V., Wehnekamp, F., Arcizet, D., Katayama, Y., Lamb, D.C., and Heinrich, D. (2013). Three-dimensional single-particle tracking in live cells: news from the third dimension. New J. Phys. *15*, 075008.

Edidin, M. (2003). Lipids on the frontier: a century of cell-membrane bilayers. Nat. Rev. Mol. Cell Biol. *4*, 414–418.

Ewers, H., Smith, A.E., Sbalzarini, I.F., Lilie, H., Koumoutsakos, P., and Helenius, A. (2005). Single-particle tracking of murine polyoma virus-like particles on live cells and artificial membranes. Proc. Natl. Acad. Sci. U S A *102*, 15110–15115.

Gao, X., Chan, W.C., and Nie, S. (2002). Quantum-dot nanocrystals for ultrasensitive biological labeling and multicolor optical encoding. J. Biomed. Opt. *7*, 532–537.

Goehring, N.W., Chowdhury, D., Hyman, A.A., and Grill, S.W. (2010). FRAP analysis of membrane-associated proteins: lateral diffusion and membrane-cytoplasmic exchange. Biophys. J. *99*, 2443–2452.

Goni, F.M. (2014). The basic structure and dynamics of cell membranes: an update of the Singer-Nicolson model. Biochim. Biophys. Acta *1838*, 1467–1476.

Goodwin, J.S., Drake, K.R., Remmert, C.L., and Kenworthy, A.K. (2005). Ras diffusion is sensitive to plasma membrane viscosity. Biophys. J. *89*, 1398–1410.

Goswami, D., Gowrishankar, K., Bilgrami, S., Ghosh, S., Raghupathy, R., Chadda, R., Vishwakarma, R., Rao, M., and Mayor, S. (2008). Nanoclusters of GPI-anchored proteins are formed by cortical actin-driven activity. Cell *135*, 1085–1097.

Groc, L., Heine, M., Cognet, L., Brickley, K., Stephenson, F.A., Lounis, B., and Choquet, D. (2004). Differential activity-dependent regulation of the lateral mobilities of AMPA and NMDA receptors. Nat. Neurosci. *7*, 695–696.

Grunwald, I.C., Korte, M., Wolfer, D., Wilkinson, G.A., Unsicker, K., Lipp, H.P., Bonhoeffer, T., and Klein, R. (2001). Kinase-independent requirement of EphB2 receptors in hippocampal synaptic plasticity. Neuron *32*, 1027–1040.

Hangen, E., Cordelieres, F.P., Petersen, J.D., Choquet, D., and Coussen, F. (2018). Neuronal activity and intracellular calcium levels regulate intracellular transport of newly synthesized AMPAR. Cell Rep. *24*, 1001–1012.e3.

Heine, M., Groc, L., Frischknecht, R., Beique, J.C., Lounis, B., Rumbaugh, G., Huganir, R.L., Cognet, L., and Choquet, D. (2008). Surface mobility of postsynaptic AMPARs tunes synaptic transmission. Science *320*, 201–205.

Hering, H., Lin, C.C., and Sheng, M. (2003). Lipid rafts in the maintenance of synapses, dendritic

spines, and surface AMPA receptor stability. J. Neurosci. *23*, 3262–3271.

Hirokawa, N., and Takemura, R. (2005). Molecular motors and mechanisms of directional transport in neurons. Nat. Rev. Neurosci. *6*, 201–214.

Hoogenraad, C.C., Milstein, A.D., Ethell, I.M., Henkemeyer, M., and Sheng, M. (2005). GRIP1 controls dendrite morphogenesis by regulating EphB receptor trafficking. Nat. Neurosci. *8*, 906–915.

Jablonski, A.E., Kawakami, T., Ting, A.Y., and Payne, C.K. (2010). Pyrenebutyrate leads to cellular binding, not intracellular delivery, of polyarginine-quantum dots. J. Phys. Chem. Lett. *1*, 1312–1315.

Jaworski, J., Kapitein, L.C., Gouveia, S.M., Dortland, B.R., Wulf, P.S., Grigoriev, I., Camera, P., Spangler, S.A., Di Stefano, P., Demmers, J., et al. (2009). Dynamic microtubules regulate dendritic spine morphology and synaptic plasticity. Neuron *61*, 85–100.

Kapitein, L.C., Schlager, M.A., Kuijpers, M., Wulf, P.S., van Spronsen, M., MacKintosh, F.C., and Hoogenraad, C.C. (2010). Mixed microtubules steer dynein-driven cargo transport into dendrites. Curr. Biol. *20*, 290–299.

Kusumi, A., Sako, Y., and Yamamoto, M. (1993). Confined lateral diffusion of membrane receptors as studied by single particle tracking (nanovid microscopy). Effects of calcium-induced differentiation in cultured epithelial cells. Biophys. J. *65*, 2021–2040.

Kusumi, A., Suzuki, K.G., Kasai, R.S., Ritchie, K., and Fujiwara, T.K. (2011). Hierarchical mesoscale domain organization of the plasma membrane. Trends Biochem. Sci. *36*, 604–615.

Kwik, J., Boyle, S., Fooksman, D., Margolis, L., Sheetz, M.P., and Edidin, M. (2003). Membrane cholesterol, lateral mobility, and the phosphatidylinositol 4,5-bisphosphate-dependent organization of cell actin. Proc. Natl. Acad. Sci. U S A *100*, 13964–13969.

Maxfield, F.R., and van Meer, G. (2010). Cholesterol, the central lipid of mammalian cells. Curr. Opin. Cell Biol. *22*, 422–429.

Maxfield, F.R., and Wustner, D. (2012). Analysis of cholesterol trafficking with fluorescent probes. Methods Cell Biol. *108*, 367–393.

Miesenbock, G., De Angelis, D.A., and Rothman, J.E. (1998). Visualizing secretion and synaptic transmission with pH-sensitive green fluorescent proteins. Nature *394*, 192–195.

Ouyang, Q., Lizarraga, S.B., Schmidt, M., Yang, U., Gong, J., Ellisor, D., Kauer, J.A., and Morrow, E.M. (2013). Christianson syndrome protein NHE6 modulates TrkB endosomal signaling required for neuronal circuit development. Neuron *80*, 97–112.

Park, M., Penick, E.C., Edwards, J.G., Kauer, J.A., and Ehlers, M.D. (2004). Recycling endosomes supply AMPA receptors for LTP. Science *305*, 1972–1975.

Penn, A.C., Zhang, C.L., Georges, F., Royer, L., Breillat, C., Hosy, E., Petersen, J.D., Humeau, Y., and Choquet, D. (2017). Hippocampal LTP and contextual learning require surface diffusion of AMPA receptors. Nature *549*, 384–388.

Renner, M., Choquet, D., and Triller, A. (2009). Control of the postsynaptic membrane viscosity. J. Neurosci. *29*, 2926–2937.

Renner, M., Schweizer, C., Bannai, H., Triller, A., and Levi, S. (2012). Diffusion barriers constrain receptors at synapses. PLoS One *7*, e43032.

Rumpel, S., LeDoux, J., Zador, A., and Malinow, R. (2005). Postsynaptic receptor trafficking underlying a form of associative learning. Science *308*, 83–88.

Rust, M.B., Gurniak, C.B., Renner, M., Vara, H., Morando, L., Gorlich, A., Sassoe-Pognetto, M., Banchaabouchi, M.A., Giustetto, M., Triller, A., et al. (2010). Learning, AMPA receptor mobility and synaptic plasticity depend on n-cofilin-mediated actin dynamics. EMBO J. *29*, 1889–1902.

Sankaranarayanan, S., and Ryan, T.A. (2000). Real-time measurements of vesicle-SNARE recycling in synapses of the central nervous system. Nat. Cell Biol. *2*, 197–204.

Saxton, M.J., and Jacobson, K. (1997). Single-particle tracking: applications to membrane dynamics. Annu. Rev. Biophys. Biomol. Struct. *26*, 373–399.

Sheffler-Collins, S.I., and Dalva, M.B. (2012). EphBs: an integral link between synaptic function and synaptopathies. Trends Neurosci. *35*, 293–304.

Simons, K., and Ikonen, E. (1997). Functional rafts in cell membranes. Nature *387*, 569–572.

Simons, K., and van Meer, G. (1988). Lipid sorting in epithelial cells. Biochemistry *27*, 6197–6202.

Singer, S.J., and Nicolson, G.L. (1972). The fluid mosaic model of the structure of cell membranes. Science *175*, 720–731.

Sun, M., Northup, N., Marga, F., Huber, T., Byfield, F.J., Levitan, I., and Forgacs, G. (2007). The effect of cellular cholesterol on membrane-cytoskeleton adhesion. J. Cell Sci. *120*, 2223–2231.

Suzuki, K.G., Kasai, R.S., Hirosawa, K.M., Nemoto, Y.L., Ishibashi, M., Miwa, Y., Fujiwara, T.K., and Kusumi, A. (2012). Transient GPI-anchored protein homodimers are units for raft organization and function. Nat. Chem. Biol. *8*, 774–783.

Suzuki, Y. (2012). Exploring transduction mechanisms of protein transduction domains (PTDs) in living cells utilizing single-quantum dot tracking (SQT) technology. Sensors (Basel) *12*, 549–572.

Triller, A., and Choquet, D. (2008). New concepts in synaptic biology derived from single-molecule imaging. Neuron *59*, 359–374.

Umemura, Y.M., Vrljic, M., Nishimura, S.Y., Fujiwara, T.K., Suzuki, K.G., and Kusumi, A. (2008). Both MHC class II and its GPI-anchored form undergo hop diffusion as observed by single-molecule tracking. Biophys. J. *95*, 435–450.

Vale, R.D., Reese, T.S., and Sheetz, M.P. (1985). Identification of a novel force-generating protein, kinesin, involved in microtubule-based motility. Cell *42*, 39–50.

Vega, A.R., Freeman, S.A., Grinstein, S., and Jaqaman, K. (2018). Multistep track segmentation and motion classification for transient mobility analysis. Biophys. J. *114*, 1018–1025.

Vermehren-Schmaedick, A., Krueger, W., Jacob, T., Ramunno-Johnson, D., Balkowiec, A., Lidke, K.A., and Vu, T.Q. (2014). Heterogeneous intracellular trafficking dynamics of brain-derived neurotrophic factor complexes in the neuronal soma revealed by single quantum dot tracking. PLoS One *9*, e95113.

Wenger, J., Conchonaud, F., Dintinger, J., Wawrezinieck, L., Ebbesen, T.W., Rigneault, H., Marguet, D., and Lenne, P.F. (2007). Diffusion analysis within single nanometric apertures reveals the ultrafine cell membrane organization. Biophys. J. *92*, 913–919.

Zhang, Q., Li, Y., and Tsien, R.W. (2009). The dynamic control of kiss-and-run and vesicular reuse probed with single nanoparticles. Science *323*, 1448–1453.

Zimmer, M., Palmer, A., Kohler, J., and Klein, R. (2003). EphB-ephrinB bi-directional endocytosis terminates adhesion allowing contact mediated repulsion. Nat. Cell Biol. *5*, 869–878.

ISCI, Volume *10*

Supplemental Information

Neuronal Receptors Display Cytoskeleton-Independent Directed Motion on the Plasma Membrane

Ruth D. Taylor, Martin Heine, Nigel J. Emptage, and Laura C. Andreae

Supplemental Figures

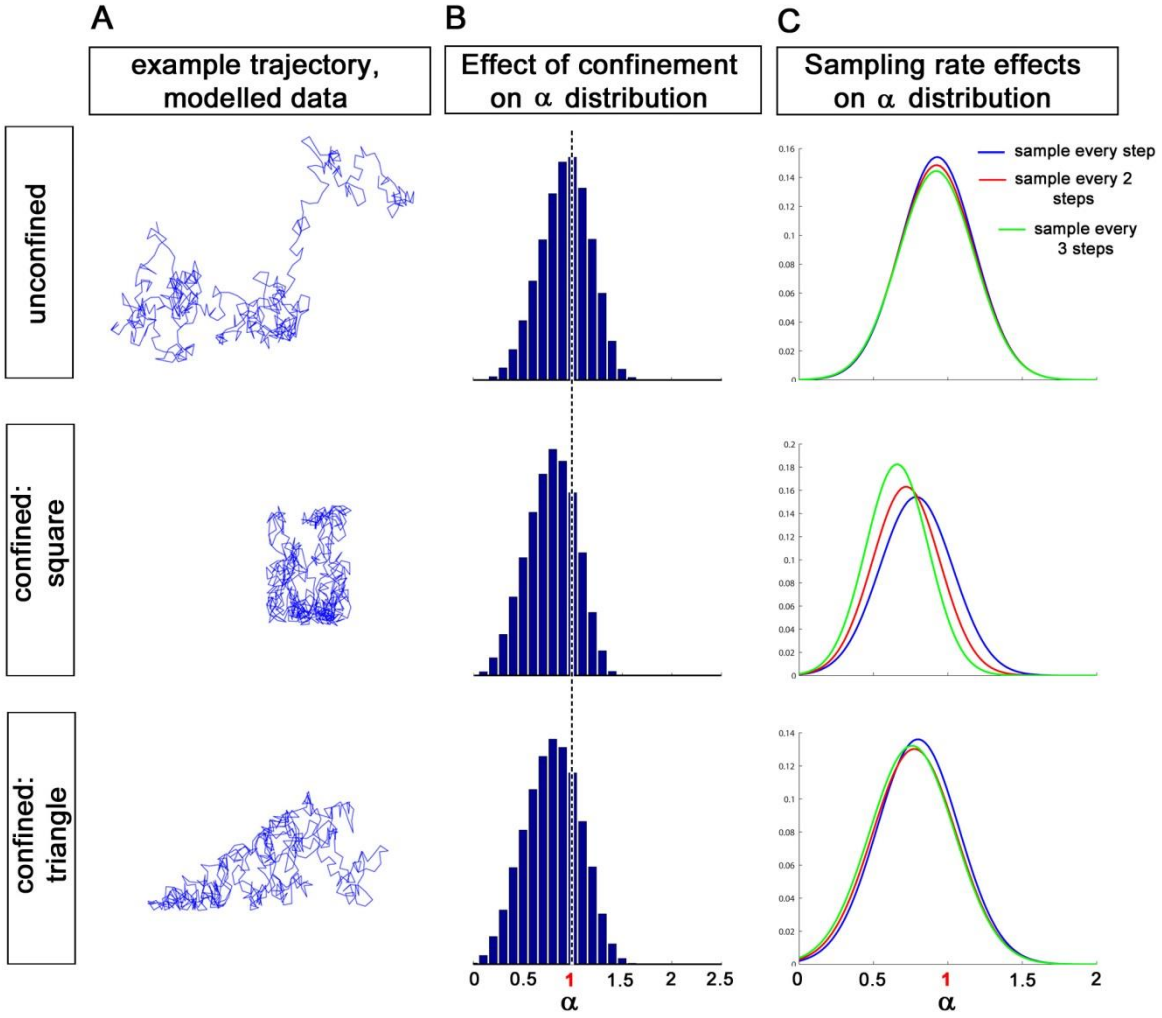

Figure S1. The effect of confinement geometry and sampling rate on motion characteristics (α) of diffusing particles. Related to Figure 2.

Particle movement modelled as diffusion, with time-resolved analysis. (**A**) Example trajectories of individual particles moving without confinement (top), within a confined square (middle) and a confined triangle where trajectory start point is in acute angle corner (bottom). (**B**) Distribution of α for each type of confinement shown in (**A**) indicates that as predicted, α peaks at 1 for unconfined movement and is shifted downwards where movement is confined. No variant in the geometry of confinement resulted in any examples of super-diffusive movement. (**C**) The effect of sampling rate on the distribution of α under different types of confinement, as shown in (**A**), indicates minimal effect on unconfined movement and a shift towards lower values of α with confinement.

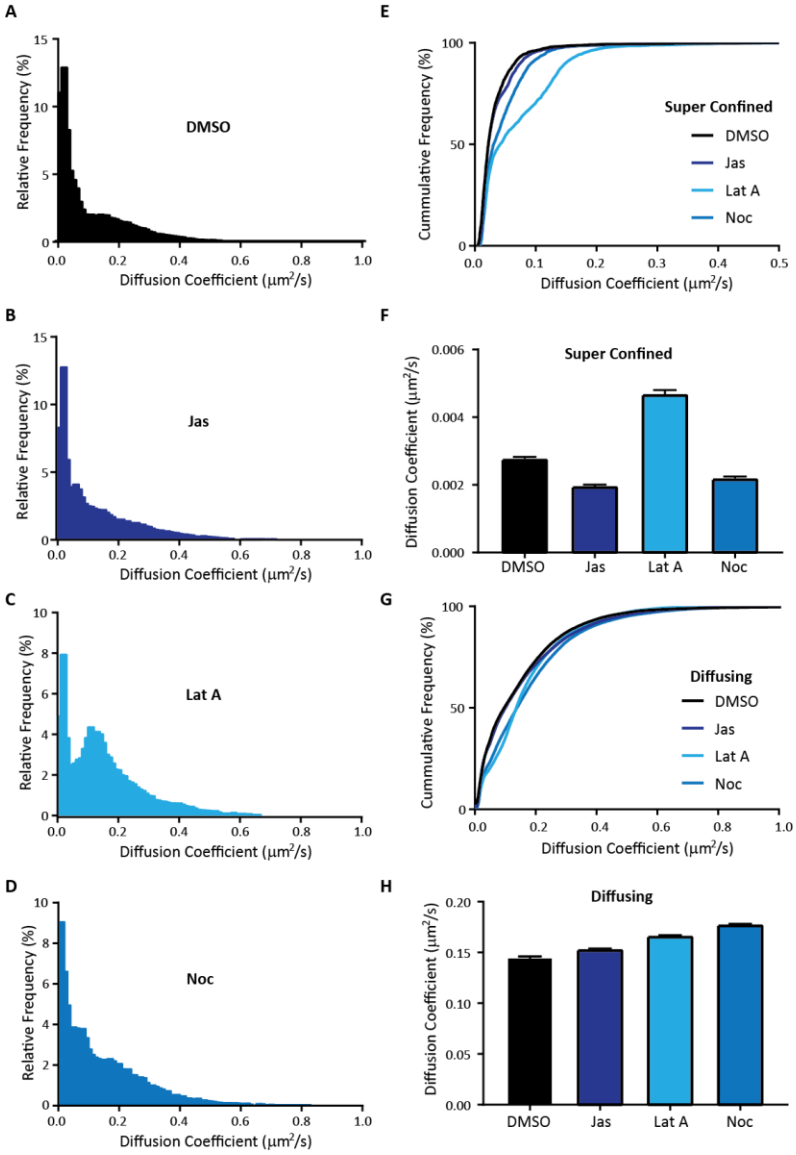

Figure S2. The effect of cytoskeletal modulatory drugs on diffusing QD-EphB2Rs. Related to Figure 3. **(A-D)** The distribution of instantaneous diffusion coefficients associated with diffusing QD-EphB2Rs in control (**A**), compared with modulating the actin cytoskeleton with 5 μM Jasplakinolide (**B**) and 5 μM Latrunculin A(**C**), or disrupting the microtubule network with 50 μM Nocodazole (**D**). The distributions were separated into two populations, super confined (**E**, **F**) and diffusing (**G**, **H**), based on a double gaussian fit to the distribution of α values that were calculated alongside the diffusion coefficient. An instantaneous diffusion coefficient was defined as belonging to a distribution if its corresponding α value was within the mean ± standard deviation for that distribution. (**E**, **G**) Cumulative frequency plots of the diffusion coefficients associated with the super confined (**E**) and diffusing (**G**) populations. (**F**, **H**) The mean of the distribution of diffusion coefficients ($\mu m^2/s$) for super confined (**F**; DMSO: 0.0337±0.0005; Jasplakinolide: 0.0366±0.0006; Latrunculin A: 0.0693±0.0012; Nocodazole: 0.0456±0.0008) and diffusing (**H**; DMSO: 0.1456±0.0004; Jasplakinolide: 0.1535±0.0004; Latrunculin A: 0.1665±0.0005; Nocodazole: 0.1778±0.0004) populations in the different cytoskeletal modulatory drugs. All distributions were significantly different from control (one way ANOVA; $p<0.0001$), error bars represent SEM.

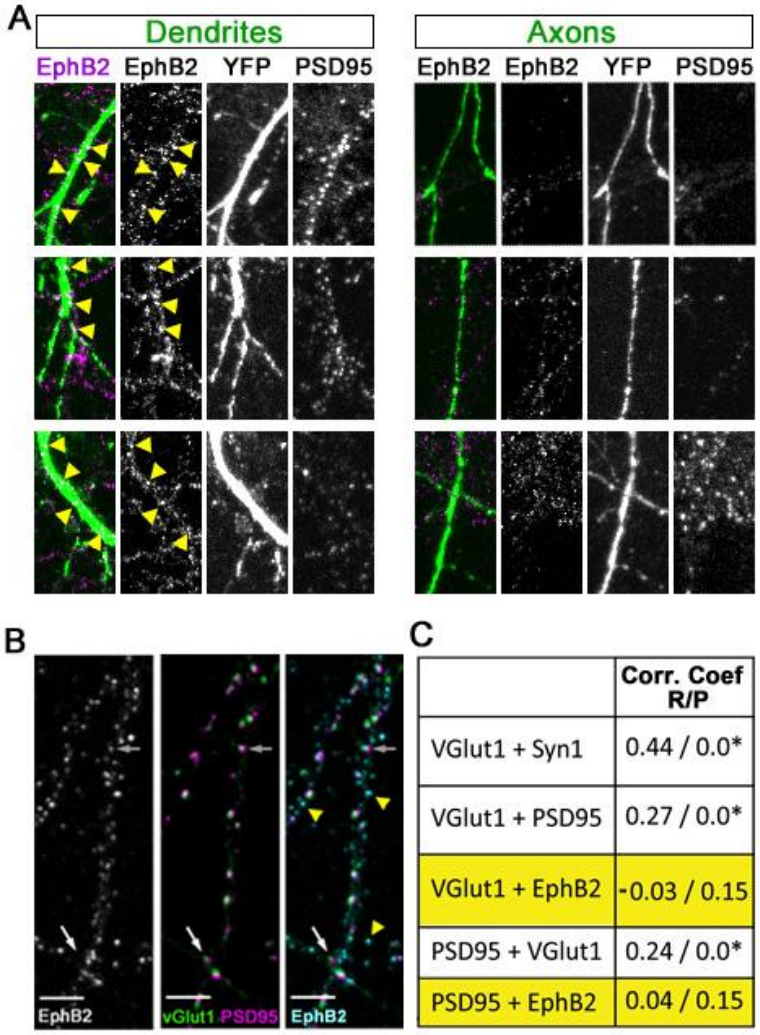

Figure S3. EphB2 Receptor localization in cultured hippocampal neurons. Related to Figure 4. (**A**) Examples of YFP-expressing dendrites (left panels) and axons (right panels) co-stained with EphB2 and PSD95 indicates that EphB2 (magenta) is predominantly found on dendrites (yellow arrowheads). (**B**) Excitatory synapses, labelled with the presynaptic marker vGlut1 (green) and postsynaptic marker PSD95 (magenta), are both EphB2 positive (grey arrow) and negative (white arrow), but the majority of EphB2 puncta (cyan) are extrasynaptic (yellow arrowheads). Scale bars 5 µm. Quantification shown in (**C**): automated puncta analysis (custom written MATLAB routines) identified labelled puncta and colocalization assessed by calculating correlation coefficients (MATLAB). As a positive control, colocalization between two known presynaptic markers, VGlut1 and synapsin1 (Syn1), showed a correlation coefficient of 0.44 ($p < 0.001$). Also significant ($p < 0.001$) with a less strong correlation was that between an excitatory presynaptic marker, vGlut1 and a postsynaptic marker, PSD95, $r = 0.27$, or $r = 0.24$ for PSD95 vs vGlut1, which should tightly overlap. In contrast, there was no correlation seen between EphB2 and vGlut1 ($r = -0.03$) nor between EphB2 and PSD95 ($r = 0.04$), indicating that EphB2 is predominantly not localized at or close to synapses.

Transparent Methods

Hippocampal Cultures and Transfection

Dissociated hippocampal neuronal cultures were prepared from embryonic day 18 Sprague Dawley rats of both sexes in accordance with all institutional and national guidelines. Hippocampi were dissociated using trypsin (5 mg/ml for 15 min at 37°C; Worthington), triturated through narrow diameter Pasteur pipettes and plated at 350 cells/mm^2 on glass coverslips pre-coated with poly-d-lysine (50 µg/ml; Sigma) and laminin (20 µg/ml). Neurons were incubated (37°C, 6% CO_2) in a 50:50 mixture of neurobasal media supplemented with B27 (2%) and neurobasal media with fetal calf serum (2%), with additional glutamax (500 µM) and penicillin-streptomycin (100 µg/ml). At 7 days *in vitro* (DIV) half of this medium was replaced with neurobasal medium plus B27 supplement. Unless otherwise specified, all culture reagents were from Gibco.

Neurons (9-10 DIV) were transfected with PSD-95-GFP or YFP (Synapsin promoter) using Effectene Transfection Reagent (QIAGEN) according to the manufacturer's instructions.

Live Single Molecule Optical Microscopy

Dissociated hippocampal neurons (10-14 DIV) were incubated for 10 minutes at 37°C in conditioned cell culture medium containing 1% casein and 1% pre-coupled QD-EphB2R mix. Pre-coupling was carried out by incubating QDot 655 (rabbit F(ab')2-anti goat IgG (H+L) conjugate (H+L); Cat no: Q11821MP, Fisher) with EphB2R antibody (BD Pharmingen) in a 1:4 ratio in sterile PBS for 1 hour at room temperature (RT). Neurons were subsequently washed and imaged in Tyrode's solution. Images were acquired <20 minutes after the staining protocol was complete.

Tyrode's solution contained: 128 mM NaCl, 5 mM KCl, 1 mM $MgCl_2$, 2 mM $CaCl_2$, 15 mM HEPES, 4 mM $NaHCO_3$, and pH was adjusted as required with HCl. NH_4Cl was used to dissipate pH gradients as previously described (Andreae et al., 2012). Temperature was maintained at 35°C for the duration of the experiments with the aid of an objective warmer and heated chamber (Harvard Apparatus). Images were acquired using an Olympus IX71 inverted microscope with a 100X, 1.4 NA oil immersion objective, coupled to a Photometrics Evolve EMCCD camera and associated Slidebook software (Intelligent Imaging Innovations, Denver). Illumination was provided by an LED emitting at 470 nm. The filter cube used for QD imaging contained a dichroic mirror at 475 nm and a 40 nm emission filter centred at 655 nm. Filters were purchased from Chroma Technologies. QD imaging movies were acquired with an acquisition rate of 32.9 Hz and were 3000 frames in length.

Electrical stimulation experiments were conducted using a field stimulation chamber (Harvard Apparatus) coupled to a SD9 stimulator delivering 900 pulses at 20 Hz. Changes in the motion of QD-EphB2Rs were analysed 5 minutes after delivery of electrical stimulation.

Filipin Fluorescence to measure Cholesterol Depletion

After treatment with methyl-β-cyclo-dextrin (1 mM, 30 mins at 37°C), dissociated hippocampal neurons (10-14 DIV) were fixed in 4% paraformaldehyde for 10 minutes and permeabilized with 0.01% saponin . Cells were then incubated with filipin (Sigma) complex (100 µg/ml) for five minutes and imaged immediately to avoid photo-bleaching.

Filipin fluorescence was measured using the ImageJ plugin: NeuronJ to trace neuronal processes, and then a custom written MATLAB (Mathworks) routine to measure the fluorescence intensity of the traced processes and subtract background from the images.

Immunostaining

Immunocytochemistry against EphB2Rs was conducted prior to cell fixation. Dissociated hippocampal neurons were blocked with casein (10%, 10 min, 37°C) and then subsequently incubated with primary antibody to EphB2R (1:500, 30 min, 37°C) and secondary antibody (1:500, 10 min, 37°C). Cells then underwent methanol fixation (100%, 1 min, -20°C) and were permeabilized (0.1% saponin, 10 min) and blocked (3% BSA, 30 min) prior to incubation with primary (1 hour at RT) and secondary antibodies (30 min at RT). The primary antibodies used were: mouse anti-PSD95 (Pierce), rabbit anti-vGLUT1 (Synaptic Systems), chick anti-GFP (Abcam).

Drugs and Reagents

Unless otherwise specified, all drugs were added to the recording chamber for 10 minutes prior to recording, dissolved in DMSO (final concentration 0.05%) and purchased from Sigma-Aldrich: methyl-β-cyclo-dextrin, filipin complex, jasplakinolide (Tocris), latrunculin A (Tocris), nocodazole and QSY-21 (Life Technologies). For experiments with low dose nocodazole (200 nM) cells were incubated in the drug for 4 hours are 37°C prior to recording.

Pre-clustered ephrinB1-Fc was obtained by incubating ephrinB1-Fc (R&D Systems) with antibodies against Fc fragments (Sigma) in a 1:10 ratio for 1hour at 37°C. The mixture was then maintained until use at 0°C. Pre-clustered ephrinB1-Fc was applied to the cells at a final concentration of 2.2 µg/ml. In control experiments Fc fragments replaced ephrinB1-Fc at an equivalent concentration.

Receptor Tracking

Initially, the shape of the point spread function (PSF) of individual QD-EphB2Rs was analysed. The change in the diameter of the PSF of individual QD-EphB2Rs over the course of an experiment was measured using the Fiji plugin Trackmate (Tinevez et al., 2017). In order to calibrate the QD-EphB2R motion in the Z plane, immobilised QDs were imaged with 100 nm step changes in focus. Individual QD-EphB2Rs where the PSF changed by more than 15% in diameter were excluded and not analysed further, this equated to <0.5 µm shift in the Z direction. The imaged molecules were detected and tracked in MATLAB using the plugin software UTrack 2.1 (Jaqaman et al., 2011). The individual QD-EphB2R tracks were then further analysed in MATLAB using custom written algorithms previously described (Arcizet et al., 2008).

Briefly, the displacement between every pair of sub-resolution co-ordinates was analysed enabling the mean squared displacement (MSD) to be calculated and the trajectory motion mode to be assigned. We calculate time resolved MSD by calculating the local MSD function over 40 frames. The local MSD function is calculated according to:

$$\Delta R2t(\delta t) = \langle(\boldsymbol{R}(t' + \delta t) - \boldsymbol{R}(t'))2\rangle - (T/2) < t' < (T/2)$$

The diffusion coefficient (D) was calculated by a linear least squares regression fit of the first three points of this function.

The motion mode is determined by fitting the power law and calculating α over the first twenty points of the MSD function:

$$\Delta R2t(\delta t) = A\delta t^{\alpha}$$

QD-EphB2Rs were determined to have a velocity when two criteria were satisfied: α greater than the critical value (1.561) and the statistical assessment of a polynomial fit to the MSD function was significantly better than a linear fit. The critical value for α was determined as being significantly greater than the α calculated for simulated random motion and is in agreement with Caspi and colleagues where a value of α>1.5 is synonymous with super diffusion (Caspi et al., 2000). Instantaneous velocity (V) was calculated for segments of a trajectory where α> 1.561 for at least two time steps.

The time resolved MSD was calculated using sliding windows of 40 steps to enable extrapolation of instantaneous motion characteristics. This enabled automatic trajectory analysis of motion modes without *a priori* segmentation.

To compare experimental data with simulated, we used trajectories without blinks and simulated 350 trajectories of similar lengths displaying random motion. The simulated trajectories were then analysed using time resolved MSD analysis and the distribution of instantaneous α obtained. The values of instantaneous α obtained for random simulated trajectories was 0.928±0.248.

Divide and conquer moment scaling spectrum (DC-MSS) analysis was conducted in MATLAB using the plugin software DC-MSS as described (Vega et al., 2018).

Data and Statistics

Unless stated otherwise in the text, all statistics are presented as the mean ± standard deviation. Statistical analysis was carried out using the Student t test, ANOVA or Chi-squared test where appropriate.

Data availability

https://data.mendeley.com/datasets/rwby5j793s/draft?a=1b88bb10-39ba-45e6-81f1-84306a39e0b4

Supplemental References

Andreae, L.C., Fredj, N.B., and Burrone, J. (2012). Independent vesicle pools underlie different modes of release during neuronal development. The Journal of neuroscience : the official journal of the Society for Neuroscience *32*, 1867-1874.
Arcizet, D., Meier, B., Sackmann, E., Radler, J.O., and Heinrich, D. (2008). Temporal analysis of active and passive transport in living cells. Physical review letters *101*, 248103.
Caspi, A., Granek, R., and Elbaum, M. (2000). Enhanced diffusion in active intracellular transport. Physical review letters *85*, 5655-5658.
Jaqaman, K., Kuwata, H., Touret, N., Collins, R., Trimble, W.S., Danuser, G., and Grinstein, S. (2011). Cytoskeletal control of CD36 diffusion promotes its receptor and signaling function. Cell *146*, 593-606.
Tinevez, J.Y., Perry, N., Schindelin, J., Hoopes, G.M., Reynolds, G.D., Laplantine, E., Bednarek, S.Y., Shorte, S.L., and Eliceiri, K.W. (2017). TrackMate: An open and extensible platform for single-particle tracking. Methods *115*, 80-90.
Vega, A.R., Freeman, S.A., Grinstein, S., and Jaqaman, K. (2018). Multistep Track Segmentation and Motion Classification for Transient Mobility Analysis. Biophysical journal *114*, 1018-1025.